Control of valley degeneracy in MoS_2 by layer thickness and electric field and its effect on thermoelectric properties

Jisook Hong,[1] Changhoon Lee,[1] Jin-Seong Park,[2] and Ji Hoon Shim[1,3,*]

[1]*Department of Chemistry, Pohang University of Science and Technology, Pohang 790-784, Korea*

[2]*Division of Materials Science and Engineering, Hanyang University, Seoul 133-719, Korea*

[3]*Department of Physics and Division of Advanced Nuclear Engineering, Pohang University of Science and Technology, Pohang 790-784, Korea*

(Received 14 July 2015; revised manuscript received 7 January 2016; published 25 January 2016)

We have investigated the valley degeneracy of MoS_2 multilayers and its effect on thermoelectric power factors. By modulating the layer thickness and external electric field strength, the hole valleys in the highest energy valence band at Γ and K points and the electron valleys in the lowest energy conduction band at K and Σ_{min} points are shifted differently. The hole valley degeneracy is observed in MoS_2 monolayer, while that of electron valley is in MoS_2 bilayer and monolayer under the external electric field. By tuning the valley degeneracy, the Seebeck coefficient and electrical conductivity can be separately controlled, and the maximum power factor can be obtained in n-type (p-type) MoS_2 monolayer with (without) the external electric field. We suggest that the transition metal dichalcogenides are good examples to investigate the role of valley degeneracy in the thermoelectric and optical properties with the control of interlayer interaction and external electric field strength.

DOI: 10.1103/PhysRevB.93.035445

I. INTRODUCTION

During the last half century, layered transition-metal dichalcogenides (TMDCs) have attracted much attention because of their characteristic quasi-two-dimensional structure and anomalous physical properties such as superconductivity [1–3] and charge density wave [4–6]. Recently, as the exfoliation technique makes it possible to obtain the monolayers of two-dimensional materials such as graphene [7], the layered TMDCs have been in the spotlight again. Especially 2H-MoS_2 and its family such as $MoSe_2$, WS_2 and WSe_2 have been studied a lot because their indirect band gap in bulk changes into direct band gap in their monolayer limit [8–12]. Because of their large direct band gap and two dimensionality, TMDCs monolayer has been applied to nano-electronics [13–15] and nano-optoelectronics [16–18].

TMDCs also have been studied as candidates for thermoelectric materials. It is known that semiconducting TMDCs have high Seebeck coefficient (S) (700–900 μV K^{-1}) [19,20] because of their characteristic quasi-two-dimensional crystal structures. Therefore, TMDCs have a possibility of high thermoelectric efficiency, which is described by the dimensionless figure of merit $ZT = S^2\sigma T/\kappa$, where σ, T, and κ represent the electrical conductivity, operating temperature, and thermal conductivity. However, the electrical conductivity of MoS_2 and its family is usually very low [19,20]; therefore, MoS_2 has been reported to have low thermoelectric efficiency ZT below 0.1 [21]. In order to improve their thermoelectric performance, it is essential to enhance their electrical conductivity while keeping the high Seebeck coefficient. There have been a few theoretical studies to enhance the thermoelectric efficiency of TMDCs by increasing their electrical conductivity. Guo *et al.* investigated the pressure effect on the electronic structure and transport properties of MoS_2. They predicted that ZT of MoS_2 can be highly enhanced under high pressure [22]. It was also suggested that the electrical conductivity and the power factor (PF) of TMDCs can be increased by making hypothetic mixed layer system such as $MoS_2/MoTe_2$ or WS_2/WTe_2 [23,24]. In these studies, they mainly focused on the increase of the electrical conductivity by reducing the band gap size. Also, Wickramaratne *et al.* [25] and Huang *et al.* [26] investigated the thermoelectric properties of multilayer TMDCs depending on their thickness by using density functional theory (DFT) calculations.

In this paper, we have focused on the control of the valley degeneracy in MoS_2 to improve thermoelectric properties. In the two bands system, total electrical conductivity and Seebeck coefficient can be described by

$$\sigma_{\text{total}} = \sigma_1 + \sigma_2 \tag{1}$$

$$S_{\text{total}} = \frac{\sigma_1 S_1 + \sigma_2 S_2}{\sigma_{\text{total}}}, \tag{2}$$

where the subscript means the band index. If we assume that the two bands are degenerate and that their contribution to the electrical conductivity is the same, the total electrical conductivity is enhanced by twice while the total Seebeck coefficient remains the same. This band convergence approach has been applied to various thermoelectric materials to enhance the PF [27,28]. In the band structures of MoS_2, we identified that there are several hole/electron valleys near the valence/conduction band edge and that their degeneracy can be severely affected by its thickness or the external electric field. We also showed that the converged valleys enhanced the electrical conductivity and the PF of MoS_2 system. We suggest that the thermoelectric properties of MoS_2 should be optimized by controlling valleys near the band gap.

II. CALCULATION DETAILS

In the calculation of the electronic structures, we used the experimental crystal structure of 2H-MoS_2, which has

*jhshim@postech.ac.kr

the space group $P6_3/mmc$ with the cell parameters of $a = 3.169$ Å and $c = 12.324$ Å. In the unit cell, Mo is at (1/3, 2/3, 1/4) and S is at (1/3, 2/3, u), where u is 0.623 [29]. For the multilayer structures, we considered bulk, four-layer, two-layer (bilayer), and one-layer (monolayer) MoS_2 structures with enough vacuum between separated multilayers.

In the first-principles calculation, we employed the full potential linearized augmented plane-wave (LAPW) method encoded in WIEN2k code [30] under the generalized gradient approximation (GGA) of Perdew-Burke-Ernzerhof (PBE) [31] using 800 k-points in the full Brillouin zone. We did not consider the spin-orbit coupling because the spin-orbit splitting does not give the significant effect on the valley degeneracy or transport properties. The effect of perpendicular external electric field has been considered in monolayer MoS_2 with the size of 0.11, 0.22, 0.33, 0.44, and 0.55 V Å^{-1}. We also compared the electronic structures of monolayer MoS_2 using frozen-core projector-augmented-wave (PAW) method, as implemented in the Vienna *Ab initio* Simulation Package (VASP) [32,33]. Consistent results were obtained for two sets of calculations in the band structures.

Transport properties were calculated using BoltzTraP code [34], which is based on the Boltzmann transport theory under the rigid band approximation and constant relaxation time approximation. Therefore, in this paper, we represented the thermoelectric properties such as S, σ/τ, and PF/τ (where τ is the relaxation time) depending on the layer thickness and external electric field. Guo *et al.* demonstrated that this approach described well the experimental Seebeck coefficient and electrical conductivity of bulk MoS_2 [21]. To ensure the convergence of the calculation, we used dense 18 000 k-points in the full Brillouin zone.

III. RESULTS AND DISCUSSION

An accurate description of the band gap is usually crucial for the transport properties of semiconductor because thermally excited charge carriers mainly contribute to the electrical conductivity. We calculated the band structures of MoS_2 using PBE-GGA and Engel-Vosko (EV)-GGA [35], which estimate the band gaps of 0.883 and 1.039 eV, respectively. Although the band gap from EV-GGA is much closer to the experimental one (1.23 eV [36]), there is no significant difference in the calculated Seebeck coefficient and electrical conductivity at the carrier concentration above $\sim 10^{17}$ cm^{-3} (see Fig. S1 of the Supplemental Material [37]). The reason is that the transport properties are mainly dominated by doped charge carriers instead of the thermally excited carriers at high carrier concentration. Because we are interested in the high carrier concentration region for the optimal thermoelectric properties, we make a case with the results from the PBE-GGA method.

A. Control of valley degeneracy by thickness or external electric field

Figure 1(a) shows the calculated band structures of MoS_2 as varying the layer thickness from bulk (infinite thickness) to monolayer. Our results are in good agreement with the reported electronic structures of bulk and multilayers of MoS_2 [9–12]. The highest valence band has hole valleys at Γ and K

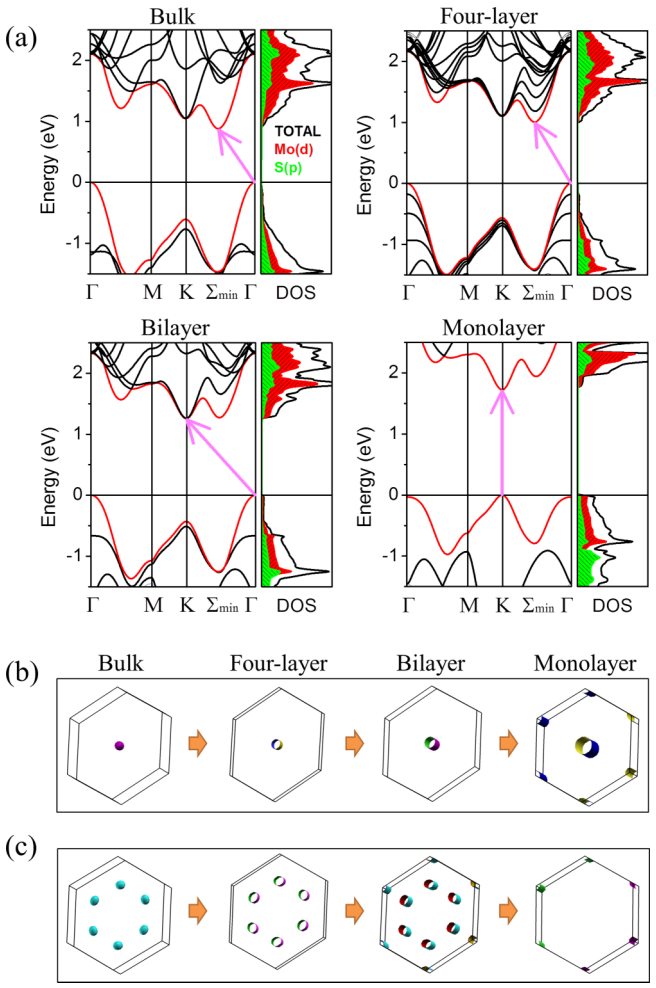

FIG. 1. (a) Band structures and density of states of bulk, four-layer, bilayer, and monolayer MoS_2. Pink arrows represent the direct/indirect band gaps. (b), (c) The constant energy surfaces in the Brillouin zone where the energy levels are below/above the valence/conduction band edge by 0.06 eV. The number of electron/hole cylinders in the Brillouin zone changes depending on the thickness of the MoS_2 multilayer.

points, and the lowest conduction band has electron valleys at Σ_{min} and K points. In bulk MoS_2, the valence band maximum (VBM) and conduction band minimum (CBM) are located at Γ and Σ_{min} points, respectively; therefore, it shows an indirect band gap of 0.883 eV. As the layer thickness reduces, the CBM at Σ_{min} shifts upward, while the VBM at Γ shifts downward, continuously. Because the bands at K point are rather robust to the change of layer thickness, monolayer MoS_2 shows the direct band gap feature at K point with the band gap size of 1.757 eV. Interestingly, the convergence of valley is shown during the evolution of layer thickness. The constant energy surfaces near the band gap edges indicate clearly the valley degeneracy, as shown in Figs. 1(b) and 1(c). In the valence band, bulk MoS_2 does not have valley degeneracy, while monolayer MoS_2 has nearly degenerate hole valleys at Γ and K points and there are three cylindrical constant energy surfaces in the Brillouin zone. In the conduction band, bulk MoS_2 has sixfold valley degeneracy at Σ_{min} point, and

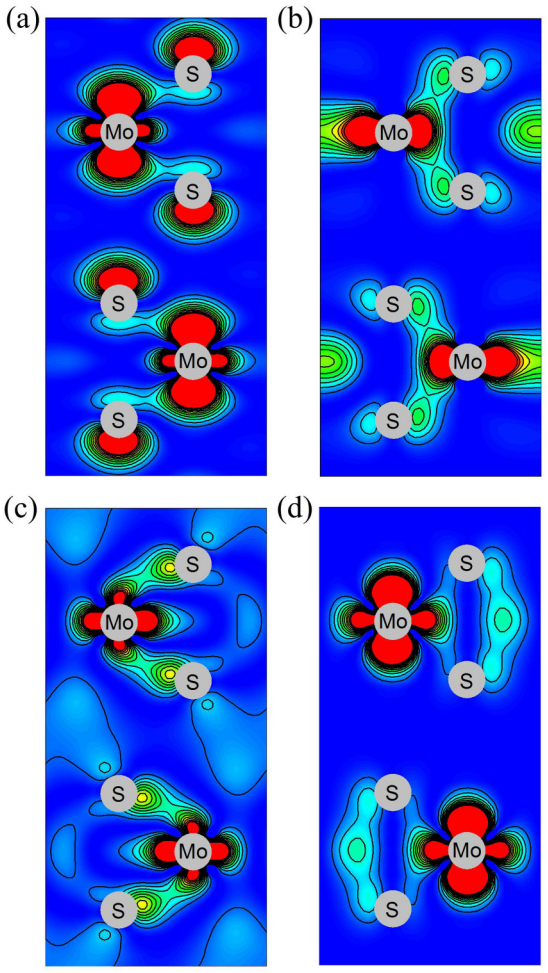

FIG. 2. The charge density of bulk MoS_2 of (a) VBM at Γ point, (b) VBM at K point, (c) CBM at Σ_{min} point, and (d) CBM at K point. Red and blue represent dense and rare charge density, respectively. Gray circles are Mo and S atoms in the unit cell. As the bulk becomes monolayer, the energy levels of VBM/CBM at Γ/Σ_{min} points are shifted up and down depending on their interlayer bonding natures.

monolayer MoS_2 has twofold valley degeneracy at K point. Note that bilayer MoS_2 shows the convergence of electron valleys at K and Σ_{min} points, thus there is a tenfold valley degeneracy. At the convergence of the valleys, the density of states is much enhanced at the band edge, and so the charge carriers are expected to be increased.

The different behavior of the valleys with the layer thickness can be understood from the different orbital characters in each valley. The hole/electron valleys near the band gap are contributed from Mo $4d$ orbital and S $3p$ orbital; their sensitivity on the layer thickness is determined by the S $3p$ orbital direction. As shown in Fig. 2, the hole/electron valleys at K point are only composed of the S p_x and p_y orbital, while the hole/electron valleys at Γ and Σ_{min} points have p_z orbital contributions. The energy levels of the hole/electron valleys at K point are not sensitive to the layer thickness or the number of neighboring layers because there is no significant interaction between the layers. However, the energy levels of hole/electron valleys at Γ/Σ_{min} points are affected as bulk MoS_2 becomes monolayer. The energy level of the hole valley at Γ point is

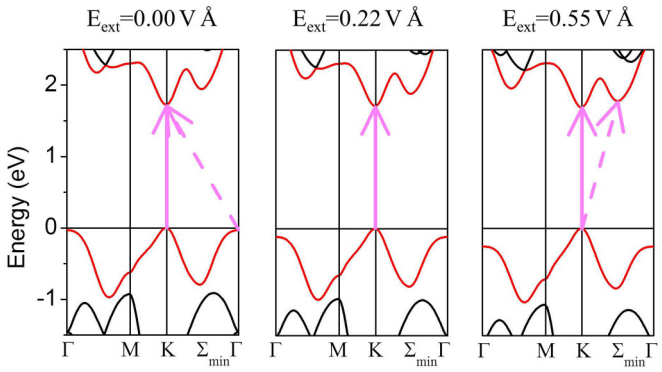

FIG. 3. Band structures of monolayer MoS_2 under the electric field of 0, 0.22, and 0.55 V $Å^{-1}$. The hole valleys at Γ and K points nearly converge without electric field, and the electron valleys at Σ_{min} and K points do converge at $E = 0.55$ V $Å^{-1}$. Pink arrows indicate the direct/indirect band gaps.

shifted down as its antibonding nature is weakened, and the energy of the electron valley at Σ_{min} point goes up as the bonding between layers is broken.

The valley degeneracy near the band gap is also adjustable by applying an external electric field, done by the control of the layer thickness. We investigated the electric field effect up to 0.55 V $Å^{-1}$, which is stronger than used in usual devices, but is possible to realize by making field-effect-transistors or sprinkling atoms/molecules on the surface [38–40]. Figure 3 shows the band structure of monolayer MoS_2 depending on the electric field strength. The valleys at Γ/Σ_{min} points are shifted downward, whereas the hole and electron valleys at K point remain robust against the field. Only the charge density of valleys at Γ/Σ_{min} points are affected from the external electric field toward z direction (see Fig. S2 of the Supplemental Material [37]). The energy difference between the hole (electron) valleys increases (decreases) approximately linearly depending on the electric field strength (see Fig. S3 of the Supplemental Material [37]). So, the valley degeneracy of valence band at K and Γ points in monolayer MoS_2 is lifted, and the VBM is shown only at K point under the electric field. In the conduction band, the valleys at K and Σ_{min} points nearly converge under the field around 0.55 V $Å^{-1}$. There is a discrepancy between CBM at K and Σ_{min} points about 80 meV. With further increased electric field, about 0.93 V $Å^{-1}$, the Σ_{min} point is expected to be the CBM. Note that the band gap properties are also changed with the modulation of valley degeneracy. The indirect band gap from Γ to Σ_{min} points in bulk MoS_2 becomes the direct band gap at K point in monolayer MoS_2. With the electric field above 0.93 V $Å^{-1}$ on monolayer MoS_2, the indirect band gap feature reappears at different momentum from K to Σ_{min} points. It will be interesting to investigate the evolution of optical properties under the control of the layer thickness and electric field.

B. Thermoelectric properties depending on valley degeneracy

The thermoelectric properties of MoS_2 multilayers are calculated along the in-plane direction. Figure 4 shows the Seebeck coefficient (S), electrical conductivity (σ/τ), and

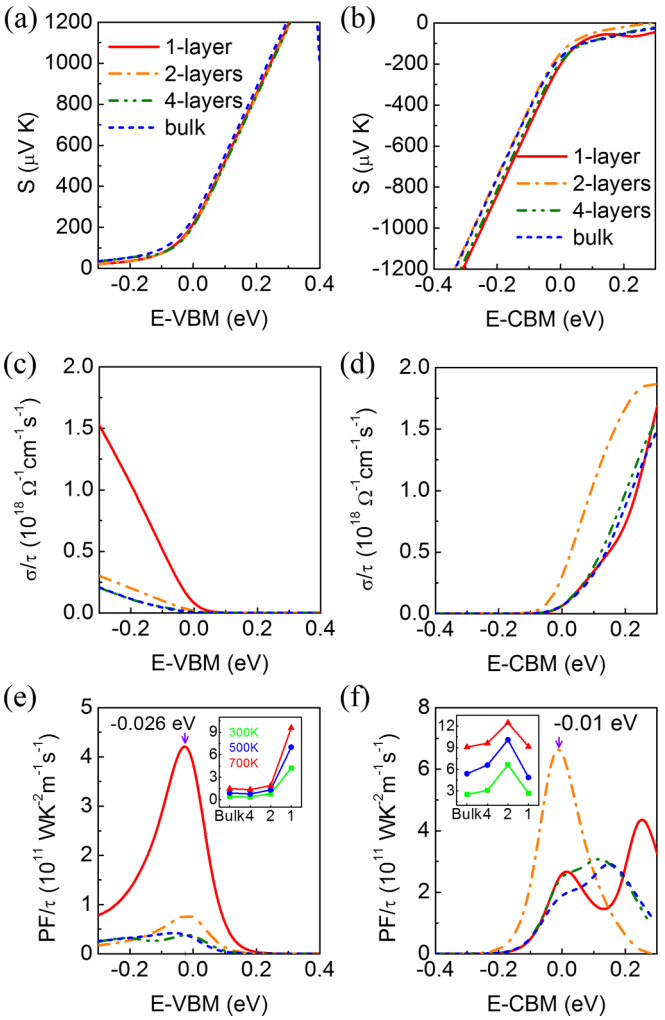

FIG. 4. In-plane Seebeck coefficient (S), electrical conductivity (σ/τ), and power factor (PF/τ) of MoS_2 at 300 K are plotted depending on their thickness and chemical potential. The left column [(a), (c), and (e)] is the property of p-type MoS_2, and the right column [(b), (d), and (f)] is that of n-type MoS_2. The chemical potential 0.0 refers to the valence and conduction band edges for p- and n-types, respectively. The insets of (e) and (f) show the maximum power factor depending on the temperature.

PF/τ of MoS_2 multilayers at 300 K. The chemical potential is represented with respect to the VBM and CBM in p-type and n-type cases, respectively. The Seebeck coefficients are not affected so much by the change of layer thickness. A small change in the Seebeck coefficient can be understood from the averaged contribution from different valleys, as indicated by Eq. (2). Dimensional dependency is not significant near the band edge because bulk MoS_2 already has two-dimensional electronic structures with weak interlayer interaction. However, the electrical conductivity shows clear changes depending on the layer thickness. Among p-type MoS_2 multilayers, monolayer MoS_2 shows significantly increased electrical conductivity as well as the PF/τ. This result is mainly caused by the valley degeneracy at the valence band edge. Similarly, among n-type MoS_2 multilayers, bilayer MoS_2 with the converged electron valleys has the highest electrical conductivity while maintaining high Seebeck coefficients. Therefore, monolayer MoS_2 and bilayer MoS_2 have the highest PF/τ when the corresponding carrier densities are $6.38 \times 10^{20}\,\mathrm{cm}^{-3}$ for p-type and $5.44 \times 10^{20}\,\mathrm{cm}^{-3}$ for n-type, respectively.

The maximum peak values of the PF/τ near the band edge as varying the temperature are shown in the inset of Figs. 4(e) and 4(f). In the whole temperature range from 300 K to 700 K, monolayer MoS_2 and bilayer MoS_2 have the best PF/τ among p-type and n-type MoS_2 multiplayers, respectively. In previous theoretical studies, the maximum ZT of the p-type bulk MoS_2 is predicted to be 0.1 at 700 K

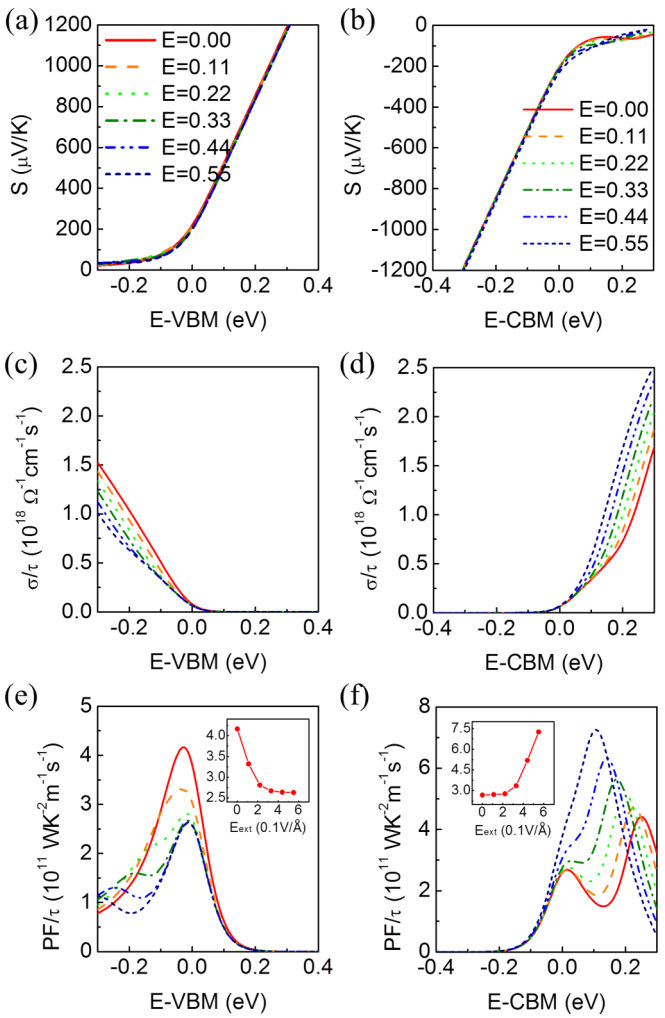

FIG. 5. In-plane Seebeck coefficient (S), electrical conductivity (σ/τ), and power factor (PF/τ) of monolayer MoS_2 at 300 K are plotted depending on the external electric field strength and chemical potential. The left column [(a), (c), and (e)] is the property of p-type monolayer MoS_2, and the right column [(b), (d), and (f)] is that of n-type monolayer MoS_2. Near the band edge, p-type (n-type) monolayer MoS_2 has maximum PF/τ when the electric field $E = 0\,\mathrm{V\,\AA^{-1}}$ ($E = 0.55\,\mathrm{V\,\AA^{-1}}$). The insets of (e) and (f) are the maximum PF/τ depending on the electric field strength. It is clearly shown that the PF/τ of p- and n-type have the opposite trend, and p-type has the maximum under $E = 0\,\mathrm{V\,\AA^{-1}}$, whereas n-type does under $0.55\,\mathrm{V\,\AA^{-1}}$.

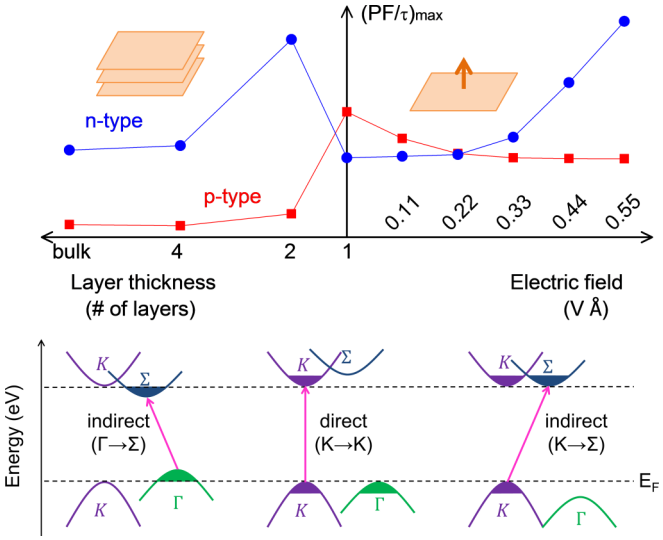

FIG. 6. Summary of valley modulation depending on multilayer thickness and external field and its effect on thermoelectric efficiency.

with a carrier concentration of $\sim 10^{20}\,\mathrm{cm}^{-3}$ [21]. According to our calculation, we suggest that six times higher ZT can be achieved in p-type monolayer MoS_2 if we assume there are no significant changes of thermal conductivity κ.

The thermoelectric properties of monolayer MoS_2 under electric field were also explored and summarized in Fig. 5. Seebeck coefficient of monolayer MoS_2 remains almost the same [Figs. 5(a) and 5(b)], and the electrical conductivity changes significantly [Figs. 5(c) and 5(d)] with the modulation of valley degeneracy, depending on the electric field strength. Similar to the study of the layer thickness, the electrical conductivity has the highest value when the valleys come close together. Even though there is an energy discrepancy of 80 meV under the field of $0.55\,\mathrm{V\,\AA}^{-1}$, because of thermal broadening, both electron valleys contribute to the transport and enhance the electrical conductivity of the n-type monolayer. The PF/τ of monolayer MoS_2 in the absence of electric field shows multiple peaks because of the contribution from K and Σ_{min} valleys with different energy levels. As those two valleys converge, the PF/τ peaks converge near the band edge, and the maximum PF/τ can be obtained [Figs. 5(e) and 5(f)]. In the case of hole doping (p-type), the valley degeneracy becomes broken with the electric field, so the PF/τ are suppressed. It could be interesting to investigate the role of the electric field on the transport and thermoelectric properties in other two-dimensional materials.

In Fig. 6, we summarize all of the discussion on the control of valley. Because of the different orbital characters, the energy level of valley is controllable by modulating multilayer thickness or external electric field. Only the valleys at Γ and Σ_{min} points are shifted upward or downward, while the valleys at K point keep almost the same energy levels. Therefore, the size of the direct band gap at K point is rather insensitive to the layer thickness and electric field, and the change of band gap is mainly induced by the hole/electron valleys at Γ and Σ_{min} points. Also, the valley degeneracy contributes greatly to optimizing the thermoelectric performance. Our results show that the thermoelectric properties are optimized when there is valley degeneracy.

IV. CONCLUSIONS

Using the *ab initio* calculation, we have investigated the thermoelectric properties of MoS_2 depending on the valley degeneracy near the band gap. The valley convergence is modulated by changing the multilayer thickness and applying perpendicular electric field. By tuning the valley degeneracy, the electrical conductivity is enhanced, while the Seebeck coefficient is not affected significantly. Also, there is a clear change of the band gap properties depending on the modulation of the valley degeneracy. Therefore, we suggest that MoS_2 and other TMDCs are good examples to use in investigating the role of valley degeneracy in the thermoelectric and optical properties.

ACKNOWLEDGMENTS

The authors thank Moon Ho Cho for fruitful discussion. This research was supported by Global Frontier Program "Global Frontier Hybrid Interface Materials" (2013M3A6B1078870) of the National Research Foundation of Korea (NRF) funded by the Ministry of Science, ICT & Future Planning, and by the National Research Foundation of Korea (NRF) grant funded by the Korea government (MSIP) (No. 2015R1A2A1A15051540).

[1] M. H. Van Maaren and G. M. Schaeffer, Phys. Lett. A **24**, 645 (1967).
[2] P. Moliniè, D. Jérome, and A. J. Grant, Philos. Mag. **30**, 1091 (1974).
[3] J. A. Woollam and R. B. Somoano, Phys. Rev. B **13**, 3843 (1976).
[4] J. A. Wilson, F. J. Di Salvo, and S. Mahajan, Phys. Rev. Lett. **32**, 882 (1974).
[5] J. A. Wilson, F. J. Di Salvo, and S. Mahajan, Adv. Phys. **24**, 117 (1975).
[6] W. L. McMillan, Phys. Rev. B **12**, 1187 (1975).
[7] K. S. Novoselov, A. K. Geim, S. V. Morozov, D. Jiang, Y. Zhang, S. V. Dubonos, I. V. Grigorieva, and A. A. Firsov, Science **306**, 666 (2004).
[8] K. F. Mak, C. Lee, J. Hone, J. Shan, and T. F. Heinz, Phys. Rev. Lett. **105**, 136805 (2010).
[9] J. K. Ellis, M. J. Lucero, and G. E. Scuseria, Appl. Phys. Lett. **99**, 261908 (2011).
[10] S. W. Han, H. Kwon, S. K. Kim, S. Ryu, W. S. Yun, D. H. Kim, J. H. Hwang, J.-S. Kang, J. Baik, H. J. Shin, and S. C. Hong, Phys. Rev. B **84**, 045409 (2011).
[11] W. S. Yun, S. W. Han, S. C. Hong, I. G. Kim, and J. D. Lee, Phys. Rev. B **85**, 033305 (2012).
[12] A. Kumar and P. K. Ahluwalia, Eur. Phys. J. B **85**, 186 (2012).
[13] B. Radisavljevic, A. Radenovic, J. Brivio, V. Giacometti, and A. Kis, Nat. Nanotechnol. **6**, 147 (2011).

[14] Y. Zhang, J. Ye, Y. Matsuhashi, and Y. Iwasa, Nano Lett. **12**, 1136 (2012).
[15] H. Li, Z. Yin, Q. He, H. Li, X. Huang, G. Lu, D. W. H. Fam, A. I. Y. Tok, Q. Zhang, and H. Zhang, Small **8**, 63 (2012).
[16] Z. Yin, H. Li, H. Li, L. Jiang, Y. Shi, Y. Sun, G. Lu, Q. Zhang, X. Chen, and H. Zhang, ACS Nano **6**, 74 (2012).
[17] H. S. Lee, S.-W. Min, Y.-G. Chang, M. K. Park, T. Nam, H. Kim, J. H. Kim, S. Ryu, and S. Im, Nano Lett. **12**, 3695 (2012).
[18] S. Jo, N. Ubrig, H. Berger, A. B. Kuzmenko, and A. F. Morpurgo, Nano Lett. **14**, 2019 (2014).
[19] L. H. Brixner, J. Inorg. Nucl. Chem. **24**, 257 (1962).
[20] R. Mansfield and S. A. Salam, Proc. Phys. Soc. B **66**, 377 (1953).
[21] H.-H. Guo, T. Yang, P. Tao, and Z.-D. Zhang, Chinese Phys. B **23**, 017201 (2014).
[22] H. Guo, T. Yang, P. Tao, Y. Wang, and Z. Zhang, J. Appl. Phys. **113**, 013709 (2013).
[23] C. Lee, J. Hong, M.-H. Whangbo, and J. H. Shim, Chem. Mater. **25**, 3745 (2013).
[24] C. Lee, J. Hong, W. R. Lee, D. Y. Kim, and J. H. Shim, J. Solid State Chem. **211**, 113 (2014).
[25] D. Wickramaratne, F. Zahid, and R. K. Lake, J. Chem. Phys. **140**, 124710 (2014).
[26] W. Huang, X. Luo, C. K. Gan, S. Y. Quek, and G. Liang, Phys. Chem. Chem. Phys. **16**, 10866 (2014).
[27] Y. Pei, X. Shi, A. LaLonde, H. Wang, L. Chen, and G. J. Snyder, Nature **473**, 66 (2011).
[28] W. Liu, X. Tan, K. Yin, H. Liu, X. Tang, J. Shi, Q. Zhang, and C. Uher, Phys. Rev. Lett. **108**, 166601 (2012).
[29] V. Petkov, S. J. L. Billinge, P. Larson, S. D. Mahanti, T. Vogt, K. K. Rangan, and M. G. Kanatzidis, Phys. Rev. B **65**, 092105 (2002).
[30] P. Blaha, K. Schwarz, G. K. H. Madsen, D. Kvasnicka, and J. Luitz, *WIEN2k, An Augmented Plane Wave + Local Orbitals Program for Calculating Crystal Properties* (Karlheinz Schwarz, Techn. Universität Wien, Austria, 2001).
[31] J. P. Perdew, K. Burke, and M. Ernzerhof, Phys. Rev. Lett. **77**, 3865 (1996).
[32] G. Kresse and J. Furthmüller, Comput. Mater. Sci. **6**, 15 (1996).
[33] G. Kresse and J. Furthmüller, Phys. Rev. B **54**, 11169 (1996).
[34] G. K. H. Madsen and D. J. Singh, Comput. Phys. Commun. **175**, 67 (2006).
[35] E. Engel and S. H. Vosko, Phys. Rev. B **47**, 13164 (1993).
[36] K. K. Kam and B. A. Parkinson, J. Phys. Chem. **86**, 463 (1982).
[37] See Supplemental Material at http://link.aps.org/supplemental/10.1103/PhysRevB.93.035445 for (i) a comparison between the transport properties based on the electronic structures using PBE-GGA and EV-GGA, (ii) a comparison between charge densities of monolayer-MoS_2 with and without the external electric field, and (iii) linear trends in energy differences between the valleys depending on the field strength.
[38] T. Hirahara, K. Miyamoto, I. Matsuda, T. Kadono, A. Kimura, T. Nagao, G. Bihlmayer, E. V. Chulkov, S. Qiao, K. Shimada, H. Namatame, M. Taniguchi, and S. Hasegawa, Phys. Rev. B **76**, 153305 (2007).
[39] T. Ohta, A. Bostwick, T. Seyller, K. Horn, and E. Rotenberg, Science **313**, 951 (2006).
[40] T. Zhang, J. Ha, N. Levy, Y. Kuk, and J. Stroscio, Phys. Rev. Lett. **111**, 056803 (2013).